One possible explanation for this discrepancy between the calculations and the cross section data is that since ^{9}Be is a deformed nucleus the coherent contribution to elastic scattering from higher-order multipoles may not be negligible. And indeed, the contributions from higher-order multipoles were found to be important in describing pion scattering from ^{9}Be.[8] Also, it has been shown in heavy-ion elastic and inelastic scattering studies that higher-order multipoles must be included in calculations to obtain an adequate description of ^{9}Be scattering from spin-zero targets.[9] We are currently investigating whether contributions from higher-order multipoles must be included in order to obtain a better description of the proton elastic data presented here.

1) C.W. Glover, P. Schwandt, H.O. Meyer, W.W. Jacobs, J.R. Hall, A.D. Bacher, C. Olmer, M. Kaitchuck, R. DeVito, IUCF Scientific and Technical Report, 1981, p. 1.

2) P. Schwandt, IUCF Report No. 81 - 3 (unpublished).

3) W. Bertozzi et al., this report p. 29.

4) H.O. Meyer, P. Schwandt, G.L. Moake, and P.P. Singh, Phys. Rev. C 23, 616 (1981).

5) P.V. Renberg, D.F. Measday, M. Pepin, P. Schwaller, B. Favier, and C. Richard-Serre, Nucl. Phys. A183, 81 (1972).

6) A. Johansson, V. Svanberg, and O. Sundberg, Arkiv for Fysik 38, 527, (1961).

7) P. Schwaller, M. Pepin, B. Favier, C. Richard-Serre, D.F. Measday, and P.V. Renberg, Nucl. Phys. A316, 317 (1979).

8) D.F. Geesaman et al., Phys. Rev. C 18, 2223 (1978).

9) V. Hnizdo, J. Szymakowski, K.W. Kemper, and J.D. Fox, Phys. Rev. C 24, 1495 (1981); V. Hnizdo, K.W. Kemper, and J. Szymakowski, Phys. Rev. Lett. 46, 590 (1981).

THE OPTICAL MODEL ANALYSIS OF 200 MeV $\vec{p}$ + ^{16}O ELASTIC SCATTERING

C.W. Glover, P. Schwandt, H.O. Meyer, W.W. Jacobs, J.R. Hall, M.D. Kaitchuck, and R.P. DeVito
Indiana University Cyclotron Facility, Bloomington, Indiana 47405

The microscopic description of a nucleon moving in a nuclear environment leads to a single-particle potential which is energy- and density-dependent. As the particle's energy increases, the single-particle potential becomes less attractive in the nuclear interior than near the nuclear surface. Thus, the single-particle potential develops a characteristic depression near the nuclear surface. We refer specifically to the treatment of the nucleon-nucleon interaction in nuclear matter in terms of a Brueckner-Hartree-Fock expansion, and its application to finite nuclei via a local density approximation.[1-3] The resulting real part of the central optical potential exhibits the same characteristic energy-dependent features as those given in the discussion above.

Phenomenological optical model analyses of elastically scattered polarized protons from ^{12}C at laboratory bombarding energies of 122, 160 and 200 MeV have shown that the real part of the central potential does indeed exhibit the energy-dependent features expected from microscopic considerations.[4,5] In Refs. 4 and 5, the central real potential had to be modified from the standard single Woods-Saxon (SWS) shape in order to obtain an adequate description of the large momentum transfer data (up to $\sim$ 5 fm^{-1}). The phenomenological modification of the real central potential consisted of adding a short-ranged repulsive

Woods-Saxon term to a longer-ranged attractive Woods-Saxon term. The resulting double Woods-Saxon (DWS) parameterization was motivated from microscopic theories[1-3] and is flexible enough to allow for a good description of the ^{12}C elastic scattering data at all three energies. The real central potential that best describes the 200 MeV ^{12}C elastic data was found to have developed a depression, making it more attractive near the nuclear surface than in the nuclear interior.

In an effort to determine if this feature of the real central optical potential is a general feature required to describe proton elastic scattering from other light nuclei or if it is unique to the A=12 system, we have measured to large momentum transfer ($q \sim 6$ fm^{-1} or $\theta_{cm} \sim 135°$) polarized proton elastic scattering from ^{16}O at 200 MeV. The cross section and analyzing power data have been analyzed in terms of the standard SWS optical model as well as in a model employing the DWS parameterization of the central real potential. The measurements are briefly described and the results of these analyses are presented in this report.

The measurements reported here were carried out using the QDDM magnetic spectrometer and the polarized beam from the Indiana University Cyclotron Facility (IUCF). The measurements were carried out in two separate run periods at IUCF. A number of overlap points provided a consistent normalization between the two run periods. The actual beam energy of the first run was 200.2 MeV, and that of the second run was 199.3 MeV.

Several self-supporting BeO, Be, and Li$_2$CO$_3$ targets were used, ranging in thickness from 15 to 104 mg/cm^2. The measurements at each angle were carried out using the BeO targets. The Be target was used to measure the Be background in the BeO spectra. The

Li$_2$CO$_3$ target served as a cross check of the BeO measurements.

The experimental setup, i.e., magnetic spectrometer and associated focal plane detector arrangement, and details about the angular acceptance, beam charge integration, and measurement of the electronic dead-time during data acquisition, were completely analogous to the 200 MeV ^{12}C experiment and are described in detail in Ref. 4.

Correction for deadtime losses (5-10%) and for the finite angular acceptance of the spectrometer (1-2%) were applied to the data. Where significant, background arising from accidental coincidences between the focal plane detector elements was determined from the spectrum, by the average number of counts above and below the elastic peak and were subtracted.

The results of the present experiment are displayed in Figs. 1-3. Numerical values are available on request from IUCF.

The optical model calculations presented here were performed using the computer code SNOOPY8.[7]

The standard optical model analysis employs the following parameterization to describe the local nucleon-nucleus potential $U(r)$:

$$U(r) = V_R f_R(r) + iW f_W(r)$$
$$+ \frac{\lambda^2}{\pi} \left[V_{so}\, g_{rso}(r) + iW_{so}\, g_{wso}(r) \right] (\vec{L} \cdot \vec{\sigma}) , \quad (1)$$

$$f_i(r) = \left\{ 1 + \exp\left[(r - r_i A^{1/3})/a_i \right] \right\}^{-1} \quad (2)$$

$$g_j(r) = (1/r)(d/dr)\left\{ 1 + \exp\left[(r - r_j A^{1/3})/a_j \right] \right\}^{-1} \quad (3)$$

The calculations using this parameterization will be labelled as 'SWS+PHEN' throughout this discussion. The meaning of this label is as follows: the central real and imaginary potentials are each parameterized by a single Woods-Saxon (SWS) form factor, and the real and
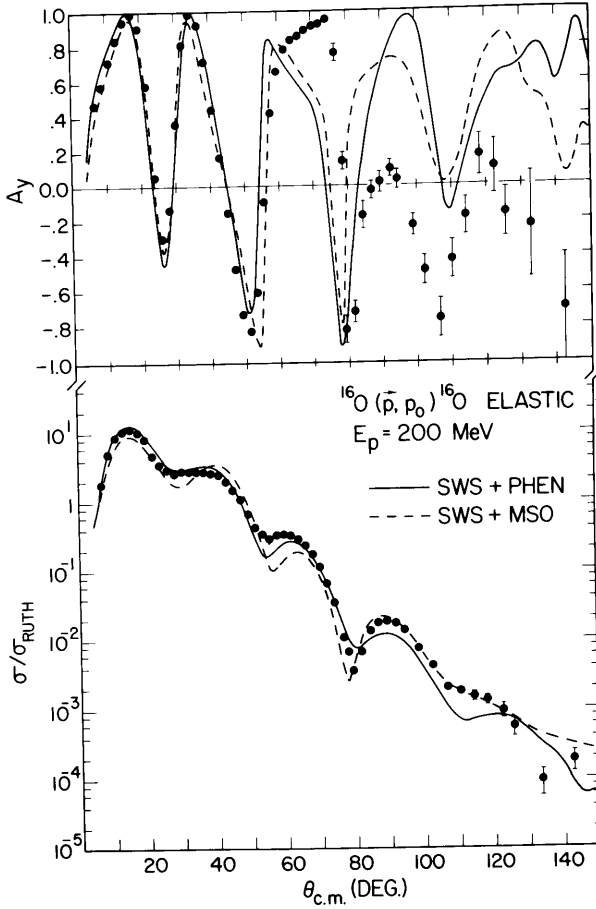
Figure 1. The elastic scattering cross section and analyzing power angular distributions for 200 MeV polarized protons from ^{16}O are displayed along with the results from optical model calculations employing the SWS parameter sets given in Table I.

Figure 2. The results from the optical model calculations employing the DWS(-) parameterization from Table II are displayed.

imaginary spin-orbit potentials are derivatives of the Woods-Saxon shapes (conventional Thomas form) and whose magnitudes (V_{so}, W_{so}) and geometrical parameters (r_j, a_j) are determined phenomenologically (PHEN) by fitting the data.

The phenomenological spin-orbit parameterization will be contrasted to the semi-microscopic spin-orbit (MSO) parameterization in which the form factors $g_{rso}(r)$ and $g_{wso}(r)$ are replaced by a common, parameter-free form factor $g_{mso}(r)$. It is easy to show[8] that a short ranged nucleon-nucleon spin-orbit interaction leads, in a microscopic framework of the

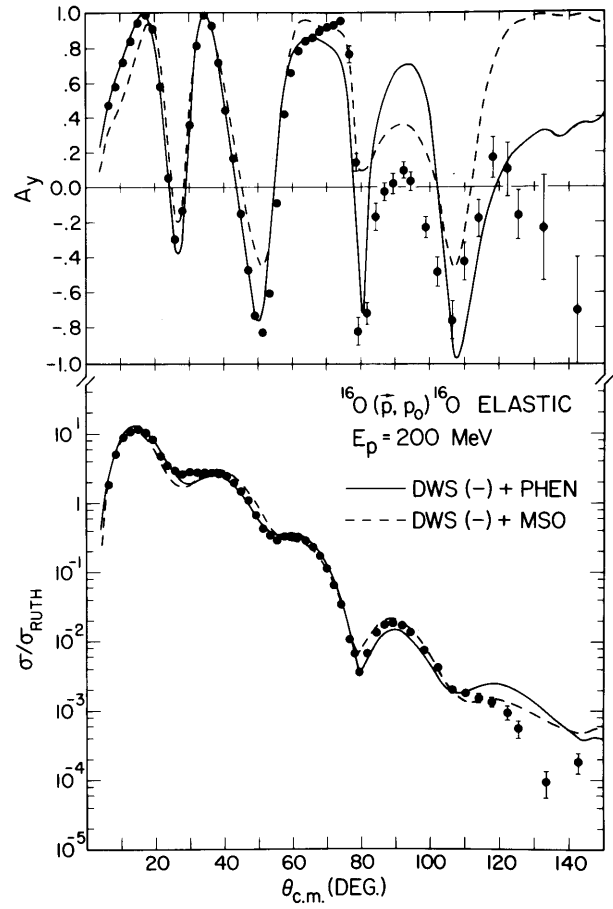optical potential, to a nucleon-nucleus spin-orbit potential which may (to very good approximation) be represented by a modified Thomas form:

$$U_{LS}(r) = C_{LS} \ (1/r) \ (d/dr) \ \rho(r) \ (\vec{L} \cdot \vec{\sigma}) \qquad (4)$$

where the constant $C_{LS} = \lambda \frac{2}{\pi} \left[V_{so} + i W_{so} \right]$ is a measure of the strength of the spin-orbit interaction, with the parameters V_{so} and W_{so} adjusted to improve the fit to the elastic data. The semi-microscopic form factor g_{so} is then given by

$$g_{mso}(r) = (1/r) \ (d/dr) \ \rho(r) \qquad (5)$$

where $\rho(r)$ represents the point nucleon density of the target nucleus. The nuclear point density $\rho(r)$ for ^{16}O that is used in the present calculations has been obtained from within the framework of the single-particle shell model which is constrained to match the experimental charge density and proton and neutron separation energies.[9] The resulting $\rho(r)$ was found to be well approximated by a sum of two Woods-Saxon forms as follows:

$$\rho(r) = 0.190 \left[1 + \exp\ (2.0r-4.9)\right]^{-1} -$$

$$0.052 \left[1 + \exp\ (3.23r-2.58)\right]^{-1} \qquad (6)$$

where r is in fm and $\rho(r)$ is in fm^{-3}. This fixes the

Figure 3. The results from the optical model calculations employing the DWS(+) parameterization from Table III are displayed.

geometrical spin-orbit parameters and only the strengths of the complex spin-orbit interaction are adjusted. Besides reducing the number of free parameters, this MSO parameterization also eliminates the unphysical singularity at the origin that plagues the Thomas form.

As discussed earlier, the real part of the central potential is expected to be less attractive in the nuclear interior than near the nuclear surface. This characteristic depression in the real part of the central potential, qualitatively predicted from microscopic derivations of the optical potential for finite nuclei in a local density approximation,[1-3] may phenomenologically be represented by a double Woods-Saxon (DWS) form, i.e, by substituting for the term $V_R f_R(r)$ in Eq. 1 the expression

$$V_R f_R(r) = V_{R1} f_{R1}(r) + V_{R2}\left[f_{R2}(r)\right]^2 \qquad (7)$$

where the potential forms f(r) are again given by Eq. 2. Note that the imaginary central potential remains unchanged (of SWS form). This shape modification introduces three new parameters. Calculations using this double Woods-Saxon form were performed and will be denoted by "DWS".

Four potential options were investigated in detail to explore separately the sensitivities of the fits to modifications of the real central and the spin-orbit potentials. The first option (SWS+PHEN) is the standard SWS parameterization with a phenomenological spin-orbit. For the second option (SWS+MSO) the semi-microscopic form factor has been used for the spin-orbit terms. In the third and fourth parameterizations, a DWS shape was taken for the real central potential, along with the PHEN or MSO spin-orbit parameterization. We shall label these last
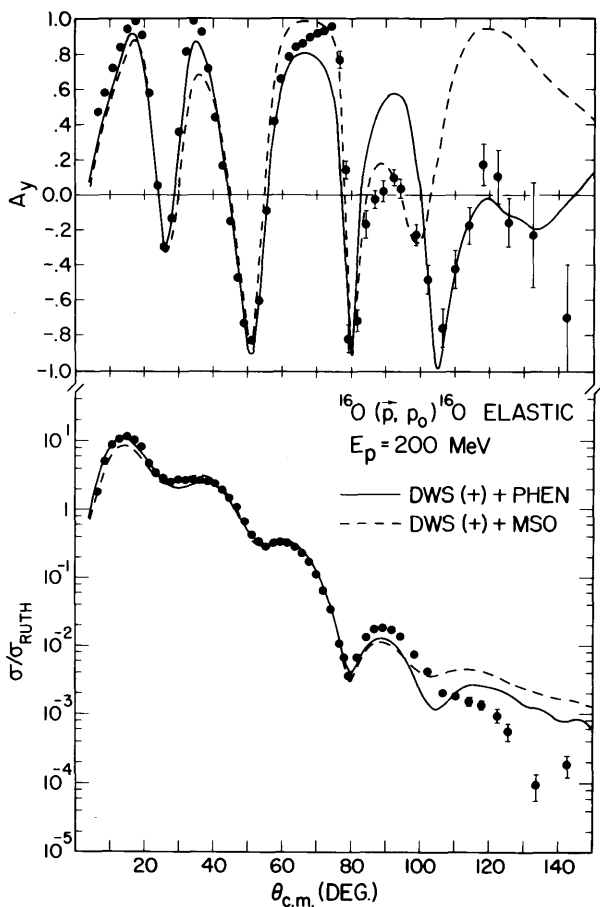
12

two optical model potential parameterizations as (DWS+PHEN) and (DWS+MSO), respectively.

The SWS optical potential parameters obtained for 200 MeV p + ^{12}C elastic scattering[4,5] and for 135 MeV p + ^{16}O elastic scattering[10] were used as starting parameters. After iterative searches on all free parameters, these two starting parameter sets converged to essentially the same 'best-fit' parameter set that is given in Table I and the corresponding fit to the elastic data is shown as a solid curve in Fig. 1. From Fig. 1, one can see that the SWS+PHEN optical potential yields cross section and analyzing power angular distributions which have the same general oscillatory structure as the data, even out to the largest angles

Table I

Parameters	SWS + PHEN	SWS + MSO	Units
V_{R1}	-9.44	-8.06	MeV
r_{R1}	1.41	1.43	fm
a_{R1}	0.60	0.584	fm
W	-18.72	-17.50	MeV
r_w	1.03	1.00	fm
a_w	0.678	0.683	fm
V_{so}	-3.767	-11.02	MeV
r_{vso}	.88	-	fm
a_{vso}	0.625	-	fm
W_{so}	2.66	10.23	MeV
r_{wso}	0.942	-	fm
a_{wso}	0.490	-	fm
χ^2_σ	6811	15920	
χ^2_{Ay}	11940	10530	
σ_R	393.3	341.0	mb
σ_{TOT}	256.6	239.3	mb

measured. The SWS+PHEN potential also provides a reasonable quantitative description of the data forward of $\theta_{cm} \sim 80°$. Beyond this angle, however, the calculated analyzing power is too large and this potential does not provide enough flux in the back-angle direction (i.e. the calculated cross section is too small).

Somewhat surprisingly, in contrast to the p + ^{12}C case, we found (see Fig. 1) that the SWS+PHEN parameter set describes the p + ^{16}O elastic scattering

data better than the SWS+MSO parameter set. The cross section calculation using the SWS+MSO parameter set does not adequately reproduce the magnitude and period of oscillation of the forward-angle ($\theta_{cm} < 80°$) data. However, for angles greater than $\theta_{cm} > 80°$, the SWS+MSO model yields an enhanced cross section which is in better agreement with the data than the SWS+PHEN calculation. In the sense that the forward-angle data are primarily sensitive to the tail region of the optical potential, whereas the far-back-angle data are more sensitive to the interior of the potential, this analysis implies that the data prefer the interior of the SWS+MSO optical potential and the tail region of the SWS+PHEN optical potential.

Next, the DWS modification (see Eq. 7) to the real part of the central optical model was tried. This DWS parameterization introduces three new parameters (V_{R2}, r_{R2}, a_{R2}) into the analysis. It was discovered that two different DWS representations of the optical potential lead to a much better description of the elastic data than does the SWS representation.

In one DWS representation of the real central potential there is an enhanced attraction (a hole) in the potential inside of 1 fm. We have denoted this DWS representation as DWS(-) and its parameter sets, calculated observables, and potentials are given in Table II, Fig. 2 and Fig. 5 respectively. Note that DWS(-) real central potential does not have the characteristic attractive pocket that was found in the 200 MeV p + ^{12}C elastic scattering analysis[4,5] and predicted by microscopic theories.[1-3]

In the other DWS representation not only does the real central potential have an attractive pocket near the nuclear surface, but it also has a sizeable repulsive core (a spike) in the nuclear interior. Here, we have labeled this DWS representation as DWS(+)
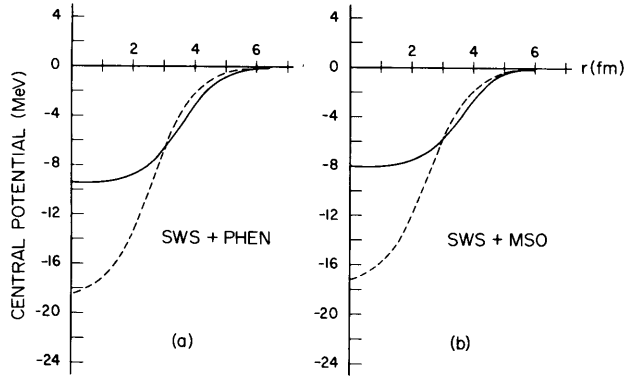
Figure 4. The SWS central real and imaginary potentials are plotted as a function of the separation distance for the phenomenological and microscopic spin–orbit parameterizations.
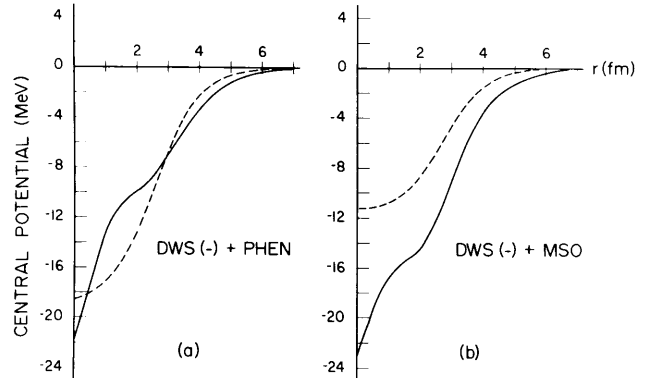

Figure 5. The SWS central real and imaginary potentials are plotted as a function of the separation distance for the phenomenological and microscopic spin–orbit parameterizations.

and its parameter sets, calculated observables, and potentials are shown in Table III, Fig. 3, and Fig. 6 respectively. The (+) and (-) signs obviously refer to the repulsive and attractive real central cores.

In comparing the cross sections calculated with the DWS(+) and DWS(-) optical potentials, one sees from Figs. 2 and 3 that both potentials adequately reproduce the data forward of $\theta_{cm} \sim 90°$. For angles greater than $\theta_{cm} \sim 90°$, the DWS(-) potential provides more particle

flux at large angles and is in better agreement with the data than is the DWS(+) optical potential. From Figs. 2 and 3 one also sees, in comparing the analyzing power calculations, the forward–angle A_y data are more accurately reproduced by the DWS(-) potential set while at back angles both potentials fit the data about equally well.

There exist at least two different potentials which employ the DWS parameterization for the real central optical potential, both leading to a much

	Table II		
Parameters	DWS(-)+PHEN	DWS(-)+ MSO	Units
V_{R1}	-170.1	-173.6	MeV
r_{R1}	0.406	0.396	fm
a_{R1}	0.819	0.812	fm
V_{R2}	+140.0	141.2	MeV
r_{R2}	0.737	0.683	fm
a_{R2}	0.898	0.836	fm
W	-19.0	-11.53	MeV
r_W	1.02	1.10	fm
a_W	0.704	0.645	fm
V_{so}	-4.22	5.135	MeV
r_{vso}	0.818	–	fm
a_{vso}	0.687	–	fm
W_{so}	2.30	11.11	MeV
r_{wso}	0.95	–	fm
a_{wso}	0.458	–	fm
χ_σ^2	2840	5829	
χ_{Ay}^2	2610	3530	
σ_R	269.0	199.1	mb
σ_{TOT}	422.6	357.3	mb

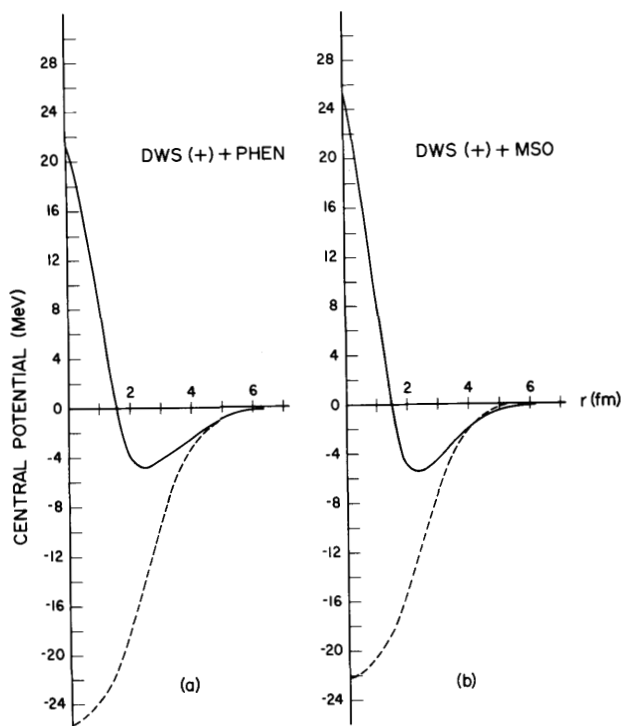|	Table III		
Parameters	DWS(+)+PHEN	DWS(+)+MSO	Units
V_{R1}	-128.4	-122.8	MeV
r_{R1}	0.88	0.812	fm
a_{R1}	0.618	0.572	fm
V_{R2}	161.5	160.9	MeV
r_{R2}	1.03	0.931	fm
a_{R2}	0.864	0.799	fm
W	-26.7	-22.9	MeV
r_W	0.983	0.949	fm
a_W	0.766	0.705	fm
V_{so}	- 3.97	-11.914	MeV
r_{vso}	0.89	–	fm
a_{vso}	0.513	–	fm
W_{so}	1.42	6.316	MeV
r_{wso}	1.05	–	fm
a_{wso}	0.607	–	fm
χ_σ^2	3957	6256	
χ_{Ay}^2	3484	8854	
σ_R	256.6	239.5	mb
σ_{TOT}	393.3	341.0	mb

Figure 6. The SWS central real and imaginary potentials are plotted as a function of the separation distance for the phenomenological and microscopic spin-orbit parameterizations.

better description of the elastic data than the SWS parameterization. Both DWS potentials give more particle flux at back angles than the SWS potential. One can readily understand, from a classical point of view, why the DWS potentials give more particle flux at back angles by considering a detector placed at some angle in the backward hemisphere. A particle can be scattered into the detector from one side of the nucleus by a large repulsive potential, or from the other side of the nucleus by a large attractive potential causing the particle to orbit around the nucleus. It is not possible from the present analysis to determine which one of these is the dominant scattering mechanism.

In the final analysis of the elastic scattering data, the semi-microscopic parameterization of the spin-orbit potential was used in place of the phenomenological parameterization for both the DWS(+) and DWS(−) central potentials. The eleven parameters were then varied and the resulting calculations and central potentials for DWS(−) + MSO and DWS(+) + MSO are shown in Figs. 2 and 3 and Figs. 5 and 6, respectively.

The conclusion from the DWS + MSO optical potential analysis is the same as that from the SWS + MSO analysis. In comparing these calculations with their phenomenological counterparts one see that the MSO parametrization does not describe the forward angle data as well as the PHEN parameterization, but there are four fewer free parameters. At the larger angles, the MSO parameterization does not make much difference in the cross section calculations. For the analyzing power calculations, the MSO parameterization makes some difference in the backward hemisphere, providing better agreement with the data at some angles and worse agreement at other angles.

We are currently investigating whether the inelastic data will prefer one DWS representation over the other by using both DWS optical potentials to generate distorted waves in the analysis of the p + ^{16}O inelastic scattering data. Our results for ^{16}O also raise the question of whether a similar ambiguity exists in the DWS parameterization of the optical potential for the ^{12}C proton elastic scattering data in Refs. 4 and 5.

1) C. Mahaux, Proc. Conf. on Microscopic Optical Potentials, Hamburg, 1978, p. 1.

2) F.A. Brieva and J.R. Rook, Nucl. Phys. A291, 299 and 317 (1977).

3) H.V. von Geramb, F.A. Brieva, and J.R. Rook, Proc. Conf. on Microscopic Optical Potentials, Hamburg, 1978, p. 104.

4) H.O. Meyer, P. Schwandt, G.L. Moake, and P.P. Singh, Phys. Rev. C 23, 616 (1981).

5) H.O. Meyer, P. Schwandt, W.W. Jacobs, and J.R. Hall, to be published.

6) P. Schwandt, H.O. Meyer, W.W. Jacobs, A.D. Bacher, S.E. Vigdor, and M.D. Kaitchuck, Phys. Rev. C 26, 55 (1982).

7) P. Schwandt, IUCF Report No. 81-3 (unpublished).

8) W.F. Hornyak, Nuclear Structure, Academic Press (1978) New York, NY, p. 248.

9) H.O. Meyer, private communication.

10) J. Kelly, Ph.D. Thesis, M.I.T. (unpublished).

THE $^{12}C(p,p')^{12}C$ REACTION AT MEDIUM ENERGIES: LARGE MOMENTUM TRANSFER AND DENSITY DEPENDENT FORCES

M. Hugi, W. Bauhoff*, and H.O. Meyer
Indiana University Cyclotron Facility, Bloomington, Indiana 47405, USA

In recent years efforts have been made to deduce a self-consistent, density-dependent, effective nucleon-nucleon (NN) interaction in the nuclear medium.[1] The success of this program became evident when it was possible to correctly predict the qualitative shape and energy dependence of the optical potential describing medium energy elastic scattering[2-5] and when it was shown that the use of a density dependent interaction improves the description of the transition between nuclear states in proton inelastic scattering.[6]

We have measured proton inelastic scattering from ^{12}C to the first excited 2^+ state in $^{12}C(E_x=4.44$ MeV). Except for the measurements at forward angles at 122 and 200 MeV[7,8], the data are a by-product of an investigation of proton elastic scattering from ^{12}C.[3-5] They constitute the most complete set of measurements on an inelastic proton scattering transition available at medium energy at present. The experiment was performed at incident lab energies of 121.9, 159.6, and 200.0 MeV using a magnetic spectrometer (QDDM). Both natural and enriched self-supporting ^{12}C targets were employed, ranging in thickness from 2 mg/cm^2 to 132 mg/cm^2. The angular range covered was from 6° to 154° in the laboratory which, e.g., at 160 MeV corresponds to a range of transferred momentum q of 50 to 1000 MeV/c.

Three ingredients enter calculations of (p,p') in the distorted-wave t-matrix approximation (DWTA): the optical potential for generating the distorted waves, the wavefunction (or the transition density) for the excited state and the effective interaction between projectile and target nucleons.

In order to study the influence of the potential generating the distorted waves on the inelastic scattering results, we have compared calculations using a standard Woods-Saxon potential with the results obtained if a non-standard shape is assumed. Here, two modifications to the conventional Woods-Saxon form have been introduced: The real central potential is given as a sum of two Woods-Saxon terms yielding a depression in the center, as predicted by microscopic theories.[1] Secondly, the spin-orbit potential (both real and imaginary parts) involves the derivative of the ground-state density distribution (obtained, e.g., from elastic electron scattering) instead of the conventional derivative of a Woods-Saxon form factor. The parameters for both these types of optical potentials are given in Ref. 5.

Since we also wanted to test the sensitivity of the results of our calculations to the transition form factor we have compared two different wave functions which are both commonly accepted. These are, on one hand, the shell-model wave function calculated